Supporting Information

Impact of N-substitution on structural, electronic, optical, and vibrational properties of thiophene-phenylene co-oligomer

V.A. Trukhanov,[ab] D. I. Dominskiy,[a] O. D. Parashchuk,[a] E. V. Feldman,[a] N.M. Surin,[c] E. A. Svidchenko,[c] M. S. Skorotetcky,[c] O. V. Borshchev[c] , D. Yu. Paraschuk[a] and A. Yu. Sosorev[ab]

[a] Faculty of Physics & International Laser Centre of Lomonosov Moscow State University, Leninskiye gory 1/62, 119991 Moscow, Russia
[b] Institute of Spectroscopy of the Russian academy of Sciences, Fizicheskaya St. 5, Troitsk, Moscow 108840, Russia
[c] Enikolopov Institute of Synthetic Polymeric Materials of Russian Academy of Sciences, Profsoyuznaya St. 70, Moscow 117393, Russia

S1. Hirshfeld surface analysis

In this Section, we provide definitions of the quantities mapped on the Hirshfeld surfaces in Fig. 4 (of the main text) and present d_{norm} and shape index maps in Fig. S1.

Fig. 4(a) shows curvedness maps at the Hirshfeld surfaces for the crystals studied. The curvedness is a function of the r.m.s. curvature of the surface: $C = \frac{2}{\pi} ln\sqrt{\kappa_1^2 + \kappa_2^2/2}$, where $\kappa_1 = -\frac{1}{|n|}\frac{\partial^2 w}{\partial u^2}$ and $\kappa_2 = -\frac{1}{|n|}\frac{\partial^2 w}{\partial v^2}$ are principal curvatures of the surface $w(u,v)$. Alongside with shape index map (Fig. S1, see below) it can be used to identify characteristic packing motifs, in particular planar stacking arrangements as discussed in the main text, and moreover the ways in which adjacent molecules contact each other.[1]

The shape index (Fig. S1(b)) is defined as $S = \frac{2}{\pi} arctan(\frac{\kappa_1 + \kappa_2}{\kappa_1 - \kappa_2})$ and represents the fine changes in the surface shape, especially in the regions with low curvature and highlights the regions where the two molecular Hirshfeld surfaces touch each other. The *S* mapping uses red and blue color schemes for complementary pairs of hollows and bumps. The front and back views of the shape index maps for CF_3-PTTP-CF_3 and CF_3-PTzTzP-CF_3 are quite similar indicating that the two sides of the molecules are involved in quite similar crystal packing. The most interesting is the area on the Hirshfeld surfaces that is simultaneously flat green on the curvedness map and is patterned by red and blue triangles touching each other on the shape index map. Such 'bow tie' pattern is a characteristic of a π…π stacking between adjacent molecules.[2] These areas are seen on the CF_3-PTzTzP-CF_3 surface (two per each side of the molecule) in Fig. S1(b).

The normalized contact distance mapped in Fig. S1(a) is defined as $d_{norm} = \frac{d_i - r_i^{vdW}}{r_i^{vdW}} + \frac{d_e - r_e^{vdW}}{r_e^{vdW}}$, where d_i and d_e are the distances from each point on the surface to the nearest nuclei inside and outside the surface, respectively; r_i^{vdW} and r_e^{vdW} are the van der Waals (vdW) radii of the corresponding atoms inside and outside the surface. Fig. S1(a) shows the associated fingerprint plots for the crystals studied. These plots give the percentage contribution

of each contacts to the total Hirshfeld surface area. Overall contributions of various types of the atoms to these plots are collated in Fig. 5 and S2.

As follows from Fig. S1(a), for CF_3-PTTP-CF_3, a lot of close contacts (red spots) include the terminal groups atoms since CF_3-PTTP-CF_3 crystal has layered structure and the molecules are inclined by approximately 66° to the ***ab***-plane. On the contrary, for CF_3-PTzTzP-CF_3, close contacts (marked as 8 and 9) appear at the edges of the surfaces; accordingly, they stabilize edge-to-edge interactions between the molecules. We suggest that this stabilized edge-to-edge interactions overwhelm the face-to-edge interaction present in CF_3-PTTP-CF_3 and trigger the crossover from the herringbone to the brickwall packing motif.

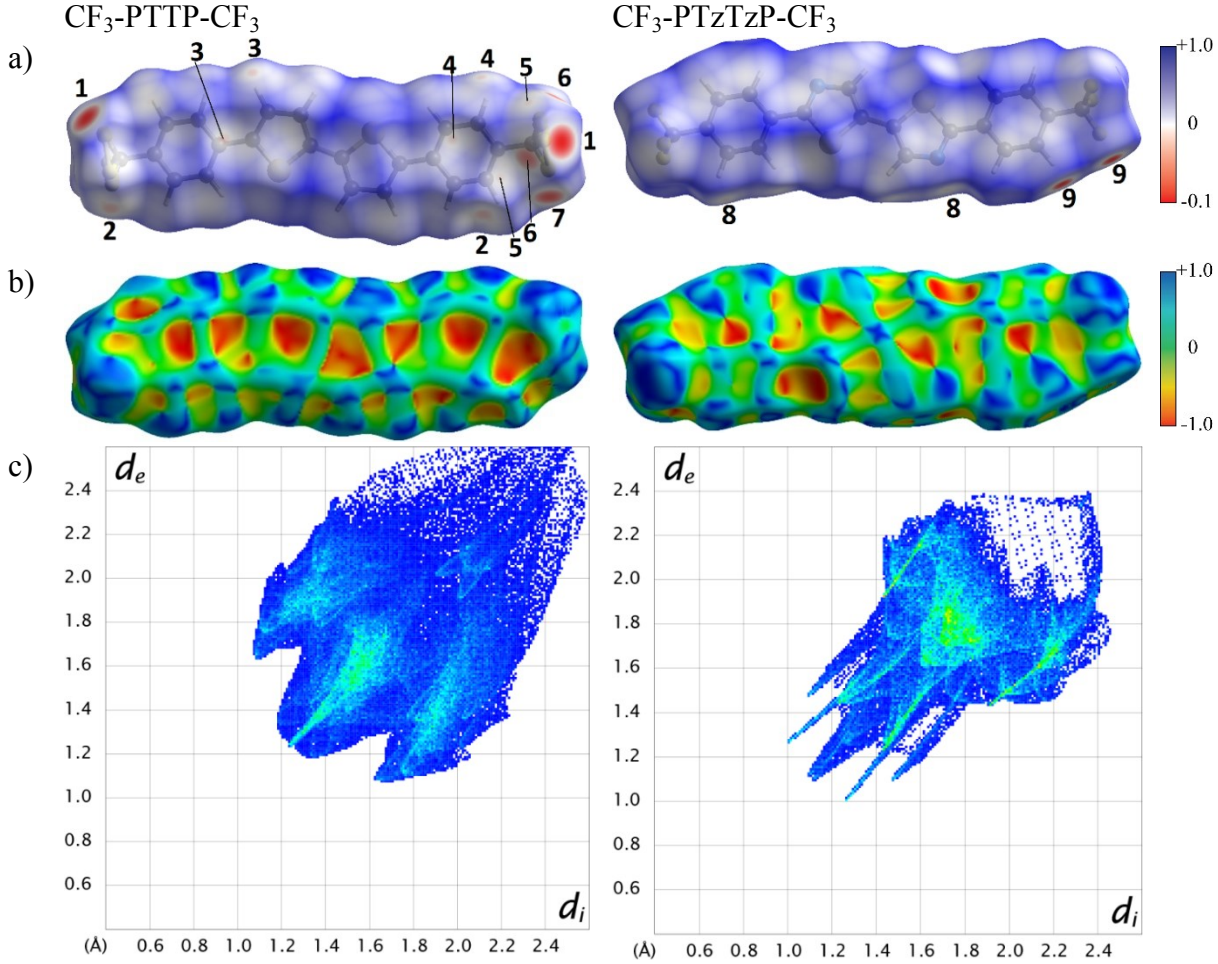

Fig. S1. Hirshfeld surfaces of CF_3-PTTP-CF_3 and CF_3-PTzTzP-CF_3 mapped with normalized contact distance (a) and shape index S (b). Red spots in (a) indicate intermolecular contacts closer than the sum of the van-der-Waals radii (close contacts), blue spots are referred to longer contacts, and contacts around the sum of van-der-Waals radii (moderate contacts) are white.[2] 2D finger print plots (c) with d_i and d_e ranging from 0.5 to 2.9 Å. For any given di and de pairs, the change in color shows the raise in occurrence: white color for no occurrence, then blue green and red for most frequent occurrence. The marked bright red regions on the surfaces are: 1 (F2,F4···F3,F5), 2 (F6···C4), 3 (H5···C7), 4 (H1···C5), 5 (F2···C4), 6 (F2···F4), 7 (F3···F3), 8 (N1···H3) and 9 (F1···H4).

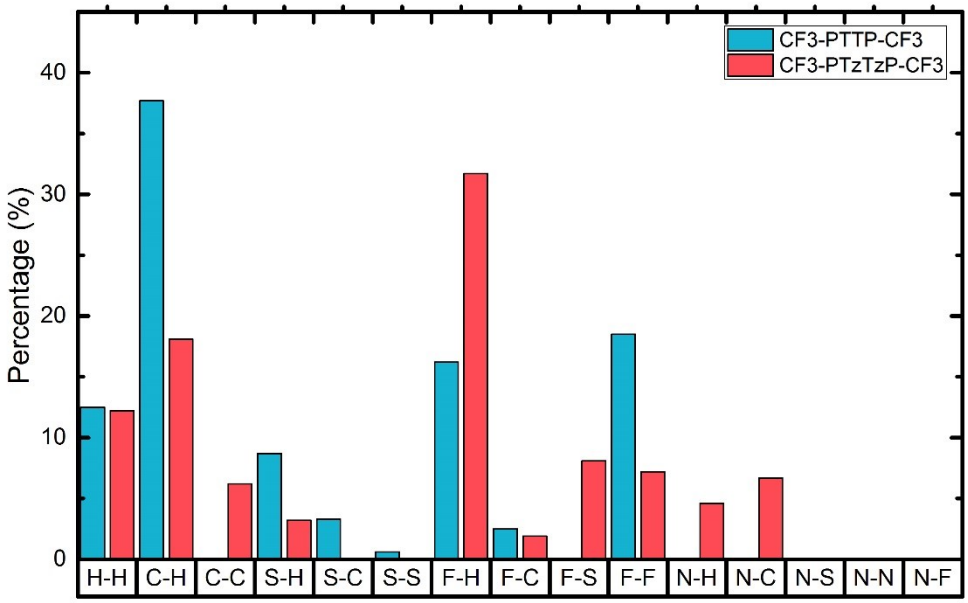

Fig. S2. Distribution of reciprocal intermolecular contacts for CF_3-PTTP-CF_3 and CF_3-PTzTzP-CF_3 arranged by atom types (b).

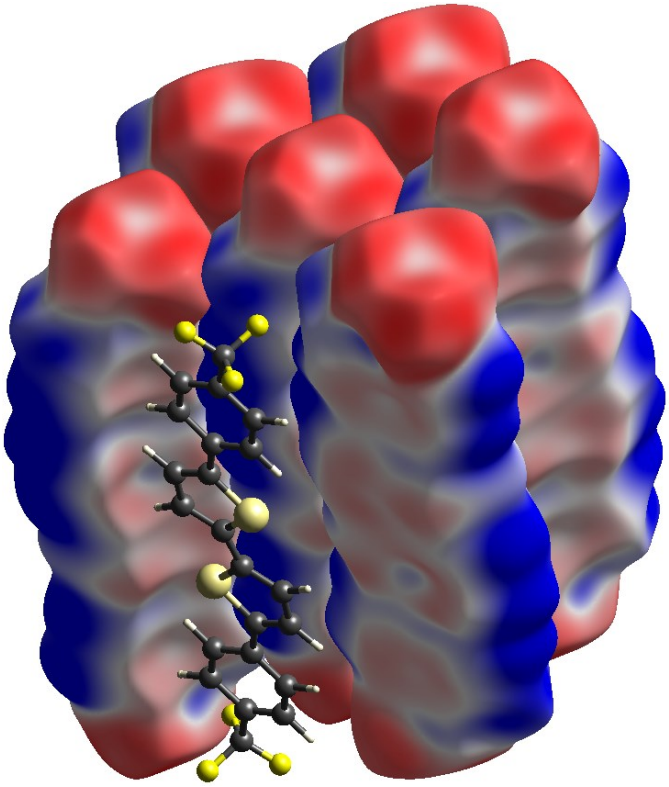

Fig. S3. ESP mapped on the Hirshfeld surfaces for a small molecular cluster in the CF_3-PTTP-CF_3 crystal. Color mapping and range for ESP as for Fig. 4.

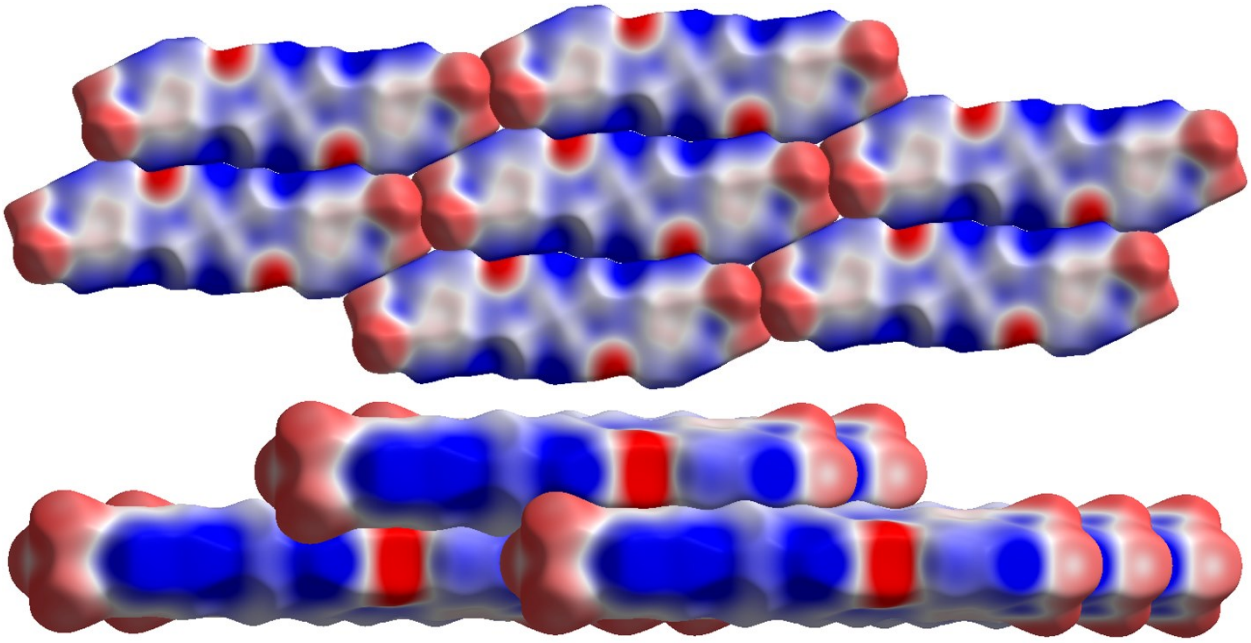

Fig. S4. ESP mapped on the Hirshfeld surfaces for a small molecular cluster in the CF_3-PTzTzP-CF_3 crystal. Color mapping and range for ESP as for Fig. 4. More information in Ref. [3].

S2. Energy framework analysis

The energy framework calculations for the studied crystals were conducted at B3LYP/6-31G(d,p) level as described in Ref. [4]. The lattice energies were estimated by summation of the interaction energies between the molecule and all the neighboring molecules within the R=25 Å distance:[10] $E_{latt} = \frac{1}{2}\sum_{R_{AB}<R} E_{tot}^{AB}$, where R_{AB} is the distance between the molecular centers, and E_{tot}^{AB} is the total interaction energy. Since all the molecules are symmetrical their molecular dipole moment is zero, and the lattice energy was estimated as the halved sum of all the interaction energies of the given molecule with all adjacent molecules.

Fig. S5 visualizes the directions of the Coulomb and dispersion intermolecular interactions. It clearly illustrates the layered structure of the CF_3-PTTP-CF_3 crystal: the intralayer interactions are much stronger than the interlayer ones. The change of the crystal structure with the N-substitution resembles that observed in Ref. [5], where fluorination of the phenyl(ene) rings also resulted in the change of the packing motif from herringbone to one- and two-dimensional π-stacking. The N-substitution facilitates edge-to-edge and face-to-face interaction between the adjacent molecules, since nitrogen atoms bear a negative charge, which attracts positively charged hydrogen atoms of the adjacent molecules stabilizing the planar (edge-to-edge) packing and hence hinders C···H contacts (edge-to-face), which are dominant in the herringbone packing (Fig. 8 in the main text).[6-10]

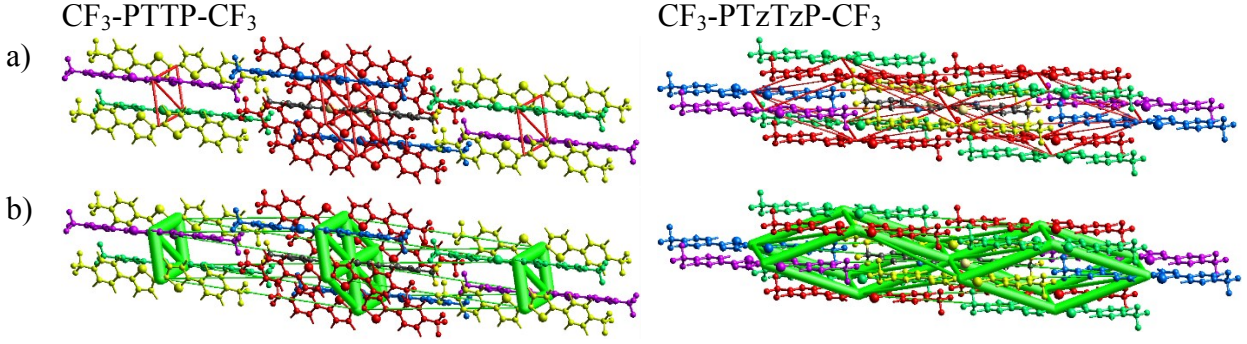

Fig. S5. Graphical representation of electrostatic interactions (the Coulomb interaction energy in red on panel a) and the dispersion energy in green on panel b) in CF_3-PTTP-CF_3 (the first column) and CF_3-PTzTzP-CF_3 (the second column) crystals. The cylinders link molecular centroids, and their thickness is proportional to the magnitude of the energy; for clarity, pairwise energies with magnitudes less than 5 kJ mol^{-1} are not shown. Details are given in Table S1-S2.

Fig. S6 summarizes contributions of dispersion, electrostatic, exchange, and polarization energies to the total lattice energy Elatt. As follows from this figure, these contributions as well as the total lattice energies Elatt are comparable for the two crystals, with Elatt slightly decreasing with the N-substitution. Fig. S7 shows convergence behavior of the CE-B3LYP lattice energies for the CF3-PTTP-CF3 and CF3-PTzTzP-CF3, plotted as partial sums including pairs of molecules within a specific radius (separation of centroids). Fig. S6 indicates that CF_3-PTzTzP-CF_3 has the lower CE-B3LYP lattice energy than CF_3-PTTP-CF_3.

Table S1. Different interaction energies of the molecular pairs for CF_3-PTTP-CF_3 in kJ mol^{-1}: N is the number of pairs, R is the distance between the molecule centroids, E_ele is the classical electrostatic energy of interaction between monomer charge distributions, E_pol is the polarization energy estimated as a sum over atoms with terms of the kind $-\frac{1}{2}\alpha|F|^2$, where the electric field F is computed at each atomic nucleus from the charge distribution of the other monomer and α are isotropic atomic polarizabilities, E_dis is Grimme's D2 dispersion correction summed over all intermolecular atom pairs, E_rep is the exchange–repulsion energy, obtained from the antisymmetric product of the monomer spin orbitals,[4] and E_tot is the total energy.

	N	R	E_ele	E_pol	E_dis	E_rep	E_tot
	4	4.89	-13.4	-2.5	-78.5	50.8	-53.0
	4	20.85	0.4	-0.1	-3.9	0.4	-2.8
	2	19.70	-2.8	-0.4	-8.5	6.4	-6.7
	2	6.15	-11.9	-2.2	-49.1	28.1	-39.6
	2	21.72	1.7	-0.2	-8.5	1.7	-4.7

Table S2. Different interaction energies of the molecular pairs for CF_3-PTzTzP-CF_3 in kJ mol^{-1}.

	N	R (A)	E_ele	E_pol	E_dis	E_rep	E_tot
	4	9.88	-8.1	-0.7	-61.4	33.7	-41.8
	2	7.38	-10.8	-3.8	-32.1	23.4	-27.8
	4	13.67	-5.3	-0.8	-21.5	11.9	-17.6
	2	21.66	1.8	-0.2	-8.7	1.4	-4.9
	2	18.58	-6.1	-0.5	-9.8	12.6	-7.6

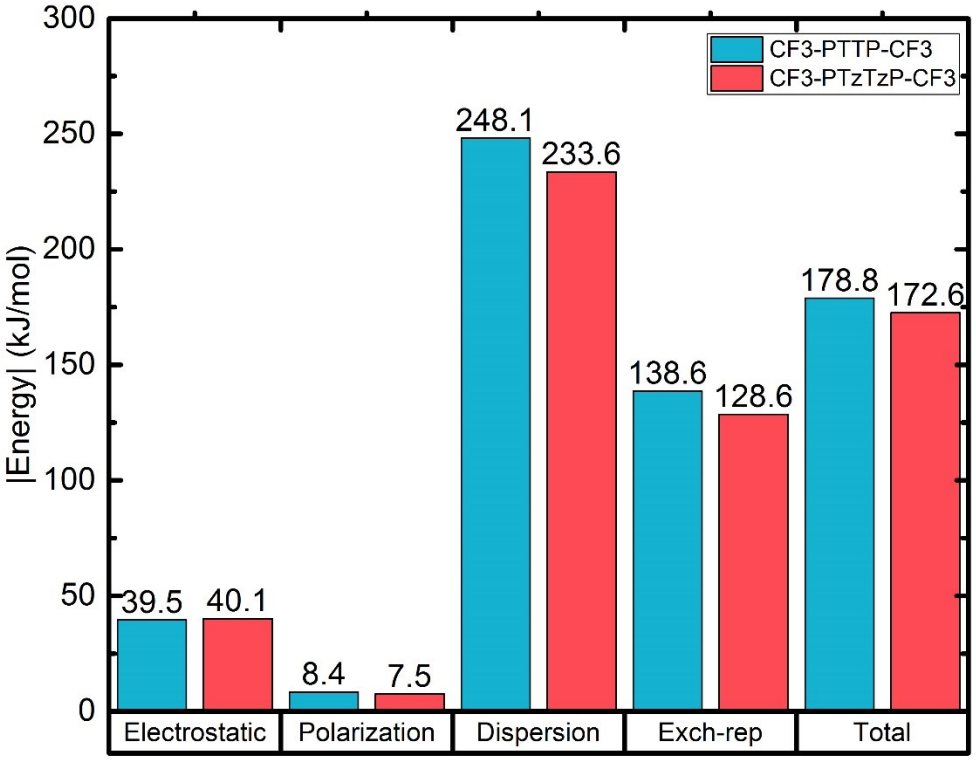

Fig. S6. Distribution of halved sum of interaction energies (absolute values) of CF_3-PTTP-CF_3 and CF_3-PTzTzP-CF_3 for a 25-Å cluster. "Total" is the total lattice energy E_{latt}.

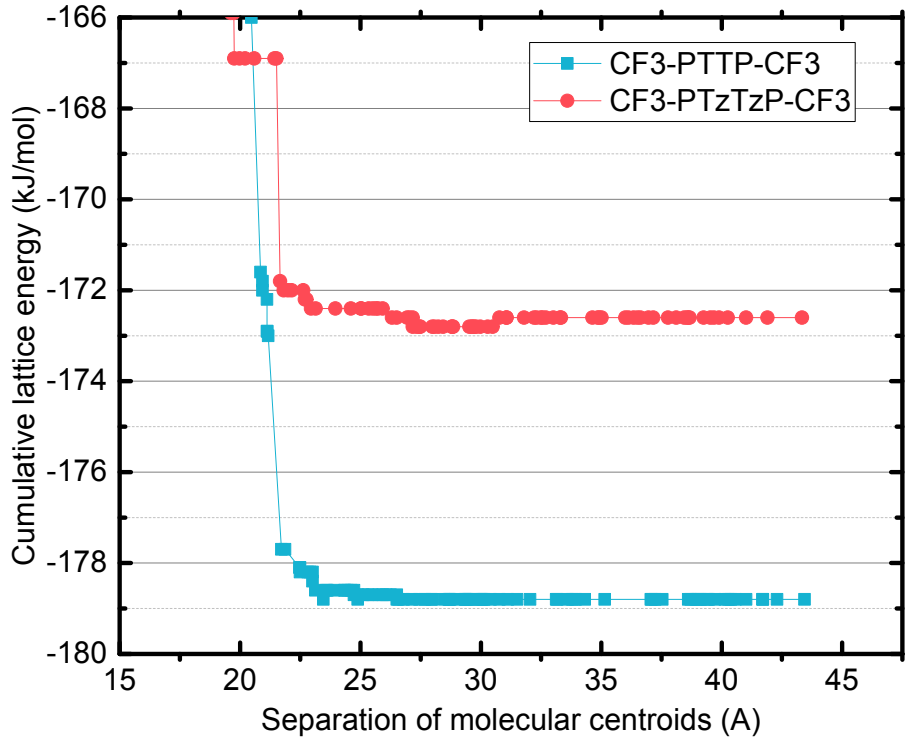

Fig. S7. Convergence of CE-B3LYP lattice energies for CF_3-PTTP-CF_3 and CF_3-PTzTzP-CF_3. The lattice energy is plotted as a partial sum against the largest separation between molecular centroids involved in that sum (at 1-A˚ intervals), and the horizontal lines are 1 kJ mol^{-1} apart.

S3. Charge mobility calculations details

Table S3. Distances (r) between the molecular centers along various directions and the corresponding electron transfer integrals (J).

CF_3-PTTP-CF_3			CF_3-PTzTzP-CF_3		
Dimer #	r, Å	J, eV	Dimer #	r, Å	J, eV
2	21.83	0.000	2	18.68	-0.000
3	19.80	-0.000	3	21.77	-0.001
4	6.19	0.082	4	7.42	-0.019
5	6.19	0.082	5	7.42	-0.020
6	19.80	-0.000	6	21.77	-0.000
7	21.83	0.000	7	18.68	-0.000
8	20.96	-0.000	8	9.93	-0.072
9	20.96	-0.000	9	13.74	-0.011
10	4.92	-0.021	10	9.93	-0.072
11	4.92	-0.024	11	13.74	-0.011
12	4.92	-0.024	12	13.74	-0.012
13	4.92	-0.021	13	9.93	-0.072
14	20.96	-0.000	14	13.74	-0.012
15	20.96	-0.000	15	9.93	-0.072

S4. Raman measurements

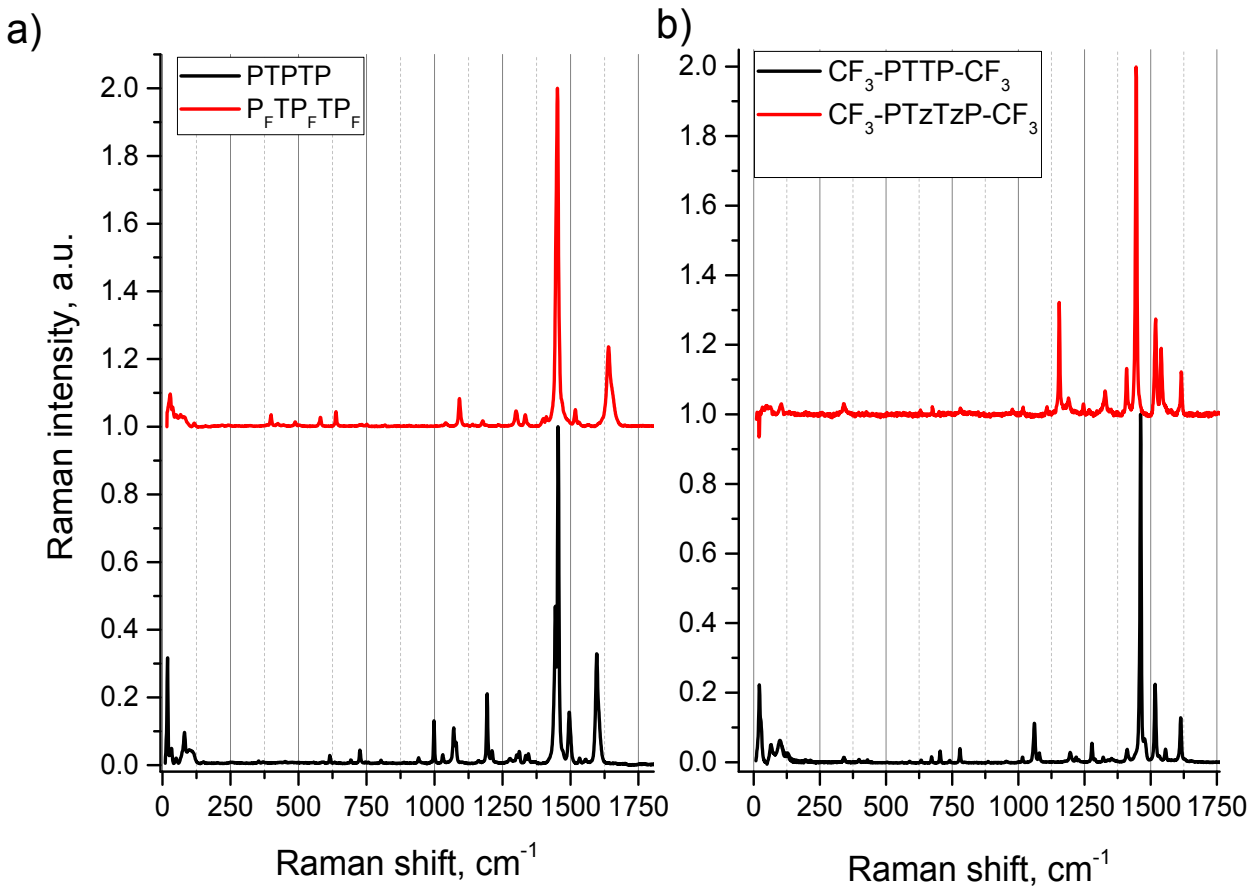

Fig. S8. Comparison of the Raman spectra of PTPTP/$P_FTP_FTP_F$ (a) and CF_3-PTTP-CF_3/CF_3-PTzTzP-CF_3 (b).

S5. OFET data

Si/SiO2 substrates with thermally-grown 200-nm thick oxide layer were sonicated in isopropanol for 15 minutes at 70°C, rinsed by isopropanol and distillated water, dried in argon flow, treated by ultraviolet radiation for 15 minutes, and treated by argon flow again. All the following stages of device preparation and characterization were conducted in inert atmosphere in argon-filled gloveboxes. A 50-nm-thick poly(methylmethacrylate) (PMMA) layer was spin-coated on the substrates at 3000 rpm from 10 mg/mL solution in toluene, and then the substrates were annealed at 70°C for 20 hours and then at 110°C for 3 hours. Hexamethyldisilazane (HMDS) self-assembled monolayer was deposited on Si/SiO_2 substrates by holding them in closed Petri dish with 0.5 ml HMDS for 20 hours at 50°C, and before deposition substrates were dipped into distillated water directly after UV treatment in order to form hydroxyl groups on SiO_2 surface. After thermal deposition in vacuum of the active layer Ca and MoO_3/Ag electrodes were evaporated through shadow masks. MoO_3/Ag layers were evaporated with some shift relatively to the Ca layer due to shadow effect, in order to allow both hole and electron-injecting electrodes have contact with active layer. The evaporation rates were 0.3 – 2.2 Å/s for Ca, 0.5 – 2.2 Å/s for MoO_3, and 4 – 10 Å/s for Ag. Thicknesses were 80 nm for Ca, 10 nm for MoO_3 and 50 nm for Ag according to the thickness monitor. For charge-mobility calculation the relative permittivity values of SiO_2 and PMMA were assumed equal to 3.9. As a gate electrode the Si substrate was used. The schematic and an image of the typical fabricated OFET are presented in Fig. S9.

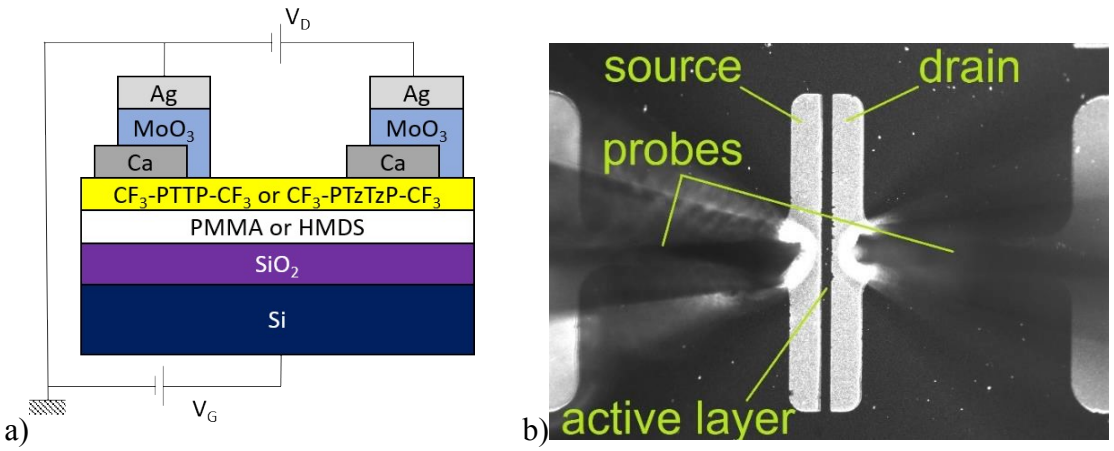

Fig. S9. OFET sample scheme (a) and its optical image (b).

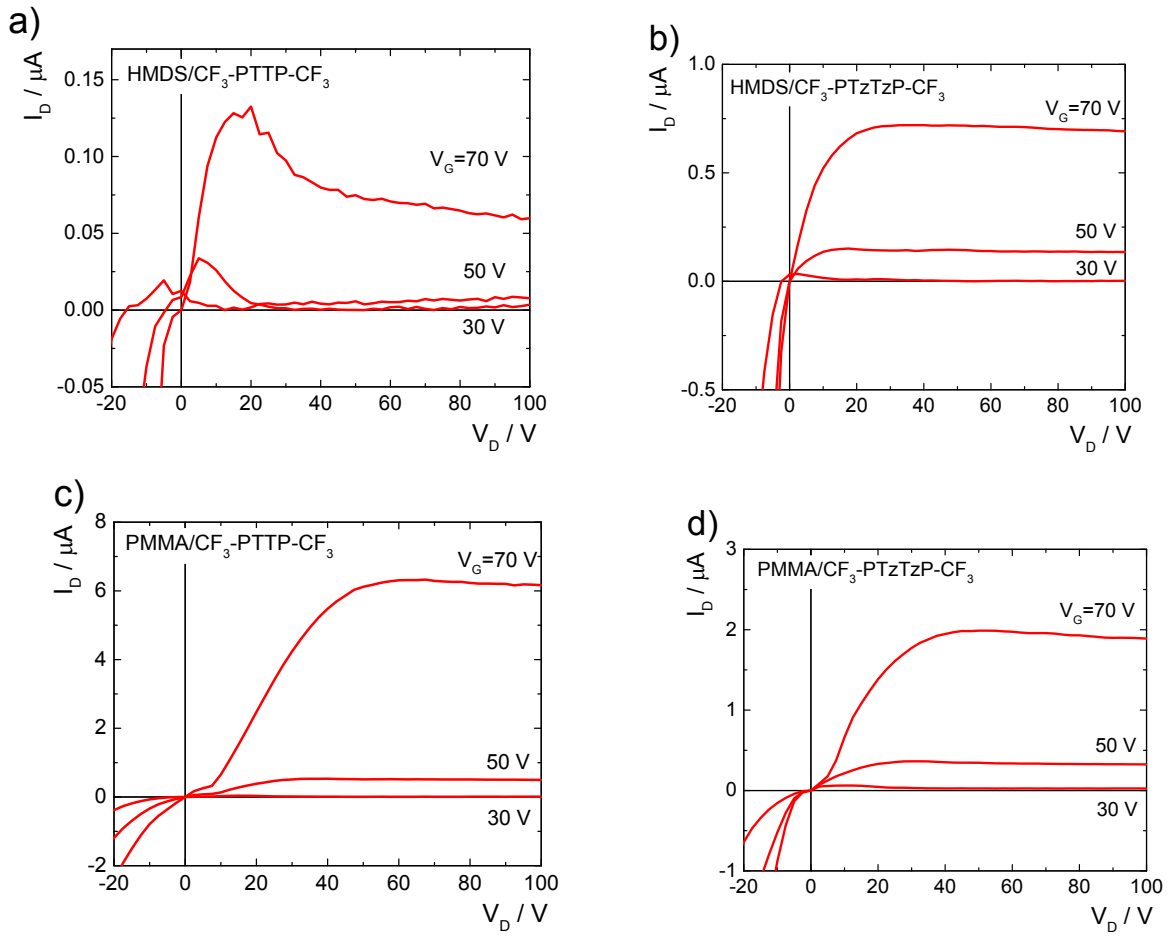

Fig. S10. Output characteristics of typical OFETs based on CF_3-PTTP-CF_3 (a,c) and CF_3-PTzTzP-CF_3 (b,d) with HMDS (a,b) and PMMA (c,d) dielectric layers. The transfer characteristics of these devices are given in Fig. 10 in the main text.

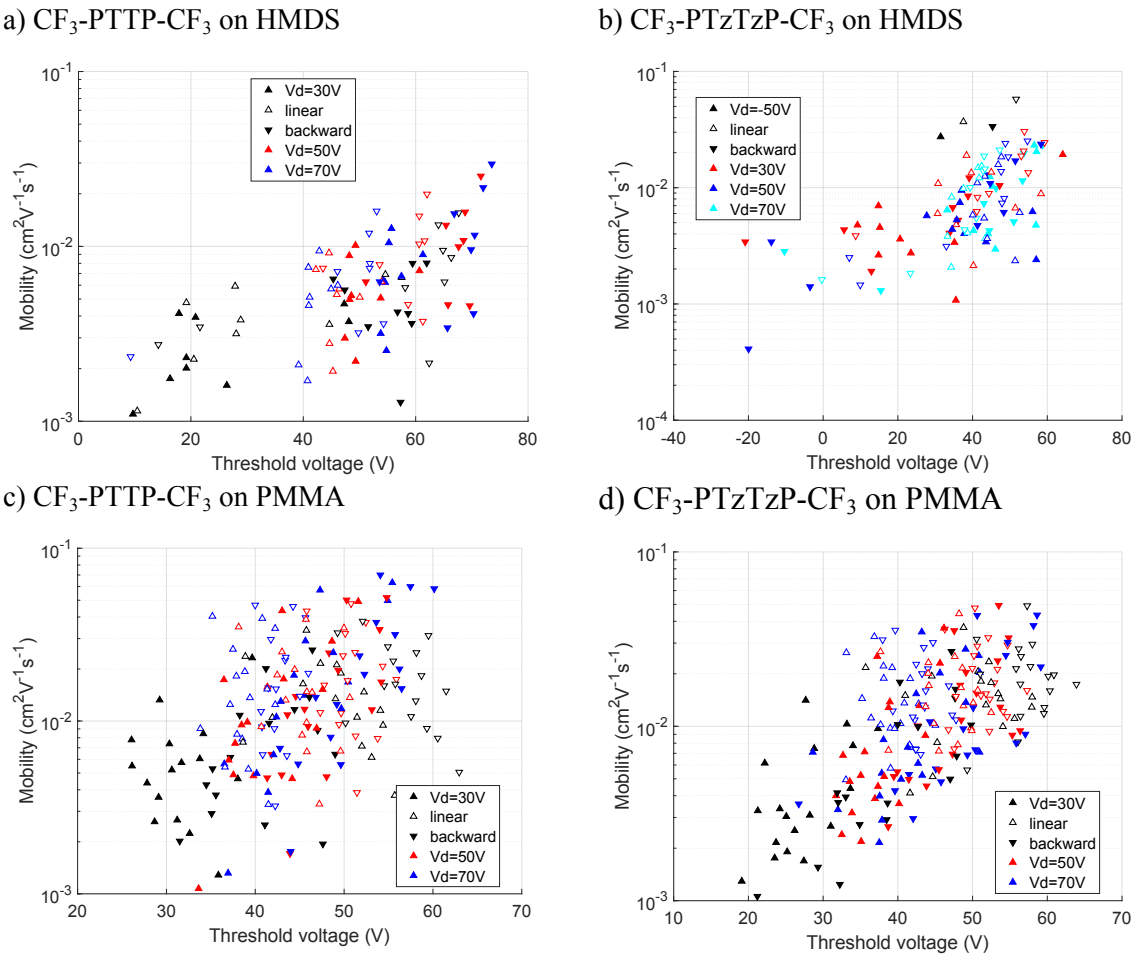

Fig. S11. Mobility vs threshold voltage diagrams for OFETs based on CF_3-PTTP-CF_3 (a,c) and CF_3-PTzTzP-CF_3 (b,d) with HMDS (a,b) and PMMA (c,d) dielectric layers.

Fig. S12 shows transfer characteristics for CF_3-PTTP-CF_3 and CF_3-PTzTzP-CF_3-based OFETs at high negative values of V_G: the drain current is within the noise level, and hence no p-type conductivity is observed.

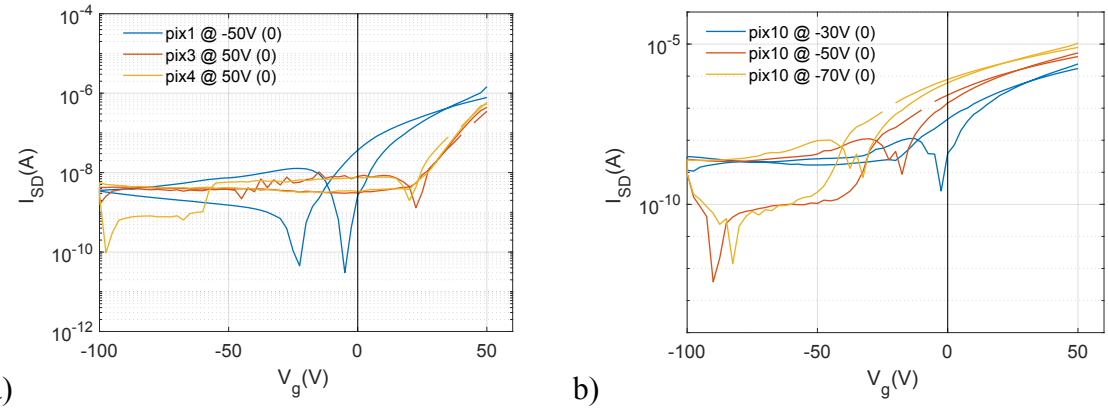

Fig. S12. Transfer characteristics in logarithmic scale at high negative values of V_G for CF_3-PTTP-CF_3 (a) and CF_3-PTzTzP-CF_3 (b) based OFETs.

For the most emissive samples with equal channel length the electroluminescence intensity for CF_3-PTTP-CF_3 was 12.55±0.12 a.u. and for CF_3-PTzTzP-CF_3 it was 2.5 higher (31.6±0.8 a.u.), the corresponding OFET images are given in Fig. S13; the images of electroluminescence recorded

in dark are colored in blue and superimposed with OFET images under backlight. The electroluminescence occurred near the hole-injecting MoO_3/Ag electrode (on the left in Fig. S13), some patches of light near the other electrode (on the right) can be attributed to reflected and scattered light. For OFETs with HMDS layers almost no measurable electroluminescence was observed.

a) 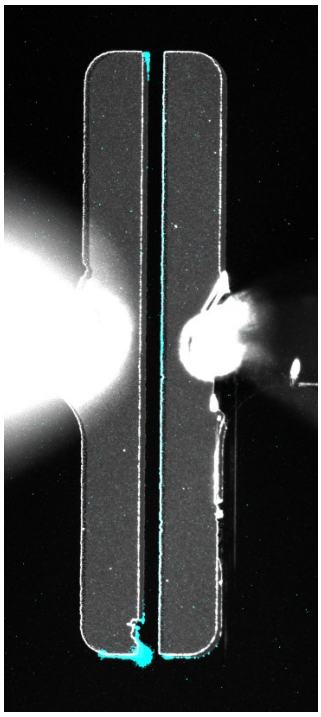 b) 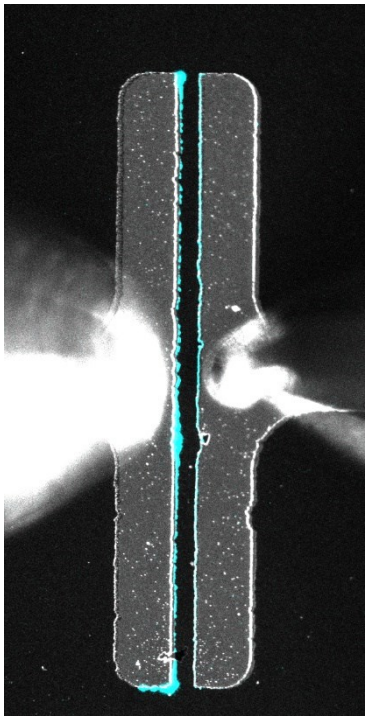

Fig. S13. Electroluminescence images of CF_3-PTTP-CF_3 (a) and CF_3-PTzTzP-CF_3 (b) based OFETs with PMMA dielectric layers, the channel lengths for both was L=30 μm.

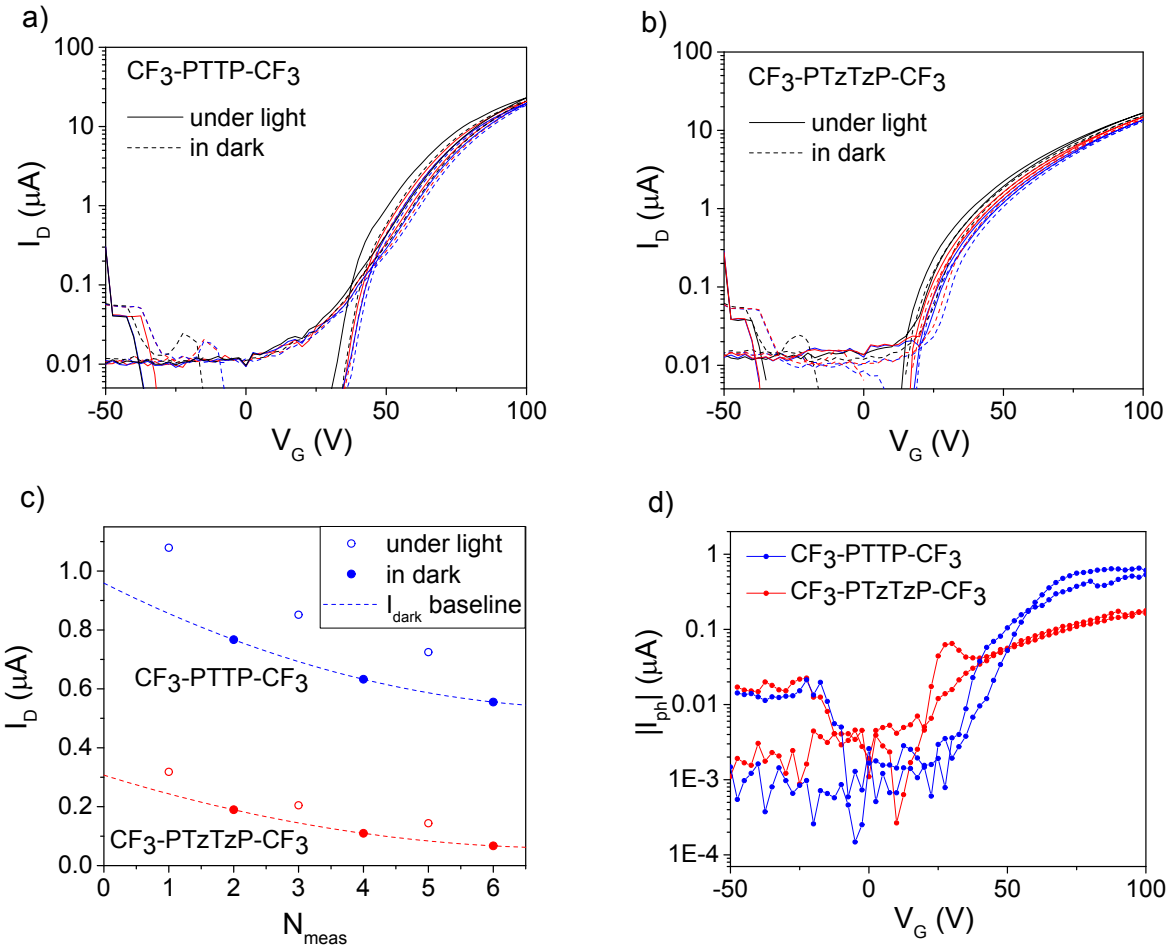

Fig. S14. Transfer characteristics under illumination and in dark for CF_3-PTzTzP-CF_3 (a) and CF_3-PTzTzP-CF_3 (b) based OFET with PMMA dielectric layers at V_D=30 V during consecutive turning on and off the incident illumination, drain current, $I_{D,}$ (V_G=57.5 V for CF_3-PTTP-CF_3 and V_G=30 V for CF_3-PTzTzP-CF_3) vs measurement serial number N_{meas} (c) and photocurrent, I_{ph}, as a function of V_G (d). Odd points (N_{meas}=1,3,5, empty dots) in panel (c) were obtained under light and even points (N_{meas}=2,4,6, full dots) were obtained in dark. The photocurrent, I_{ph} , was calculated for each V_G as an average over three values of differences between I_D under light and in dark (the baseline dark current); the latter was taken in order to take into account OFET degradation during the measurements.

S6. AFM images of polycrystalline thin films surface

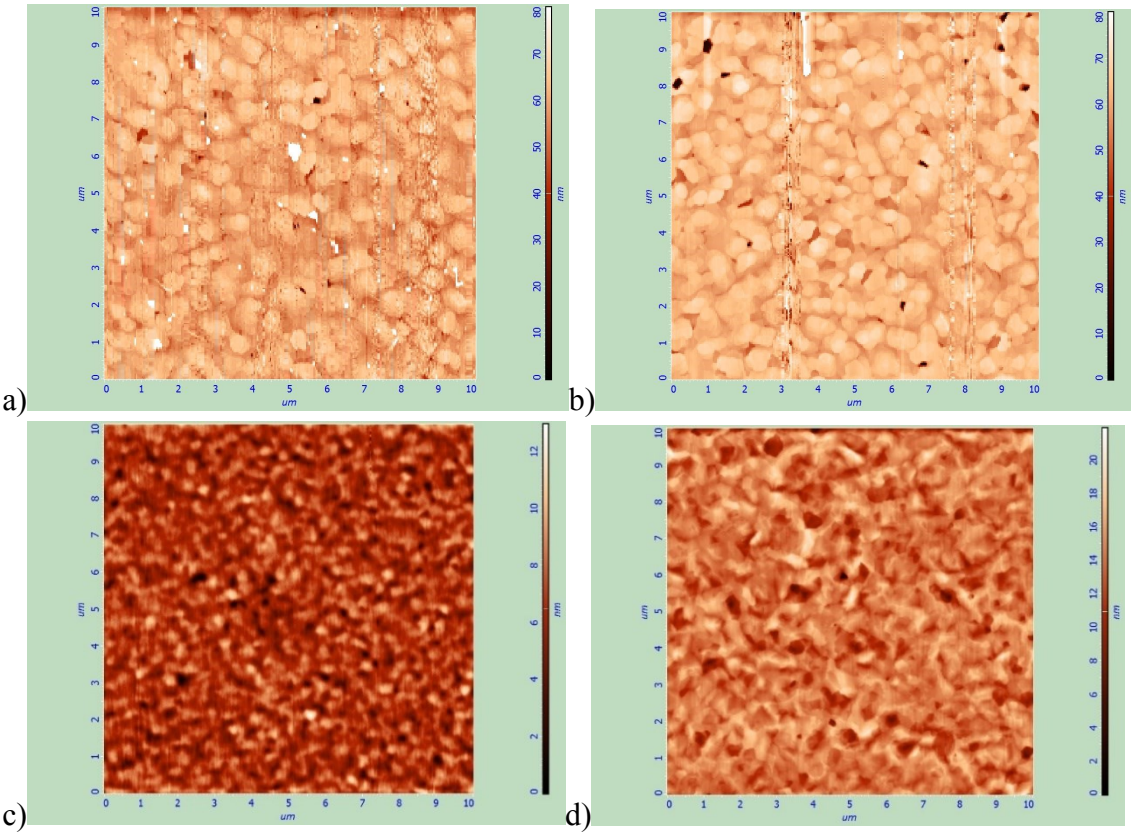

Fig. S15. 10x10 μm AFM images of CF_3-PTzTzP-CF_3 (a,c) and CF_3-PTTP-CF_3 (b,d) on HMDS (a,b) and PMMA (c,d). Average roughness is 3.94 nm (a), 3.28 nm (b), 1.07 nm (c) and 1.46 nm (d).

References

1. J. J. McKinnon, M. A. Spackman and A. S. Mitchell, *Acta Cryst. B*, 2004, **60**, 627.

2. J. J. McKinnon, D. Jayatilaka and M. A. Spackman, *Chem. Commun*., 2007, 3814.

3. A. J. Edwards, C. F. Mackenzie, P. R. Spackman, D. Jayatilaka and M. A. Spackman, *Faraday Discuss*., 2017, **203**, 93.

4. C. F. Mackenzie, P. R. Spackman, D. Jayatilaka and M. A. Spackman, *IUCrJ*, 2017, **4**, 575.

5. A. Yu. Sosorev, V. A. Trukhanov, D. R. Maslennikov, O. V. Borshchev, R. A. Polyakov, M. S. Skorotetcky, N. M. Surin, M. S. Kazantsev, D. I. Dominskiy, V. A. Tafeenko, S. A. Ponomarenko and D. Yu. Paraschuk, *ACS Appl. Mater. Interfaces*, 2020, **12**, 9507.

6. Y. Krupskaya, M. Gibertini, N. Marzari and A.F. Morpurgo, *Adv. Mater*., 2015, **27**, 2453.

7. E. O. Levina, I. Y. Chernyshov, A. P. Voronin, L. N. Alekseiko, A. I. Stash and M. V. Vener, *RSC Adv*., 2019, **9**, 12520.

8. X. P. Cui, C. Y. Xiao, W. Jiang and Z. H. Wang, *Chem. Asian J*., 2019, **14**, 1443.

9. M.-H. Yoon, A. Facchetti, C. E. Stern and T. J. Marks, *J. Am. Chem. Soc*., 2006, **128**, 5792.

10. S. E. Koh, B. Delley, J. E. Medvedeva, A. Facchetti, A. J. Freeman, T. J. Marks and M. A. Ratner, J. Phys. Chem. B, 2006, **110**, 24361.